JOURNAL OF GEOPHYSICAL RESEARCH, VOL. 94, NO. D6, PAGES 8549-8565, JUNE 20, 1989

Atmospheric Carbon Dioxide at Mauna Loa Observatory 2. Analysis of the NOAA GMCC Data, 1974-1985

KIRK W. THONING AND PIETER P. TANS

Cooperative Institute for Research in Environmental Sciences, University of Colorado, Boulder

WALTER D. KOMHYR

Air Resources Laboratory, National Oceanic and Atmospheric Administration, Boulder, Colorado

The first 12 years (1974-1985) of continuous atmospheric CO_2 measurements from the NOAA GMCC program at the Mauna Loa Observatory in Hawaii are analyzed. Hourly and daily variations in the concentration of CO_2 due to local sources and sinks are described, with subsequent selection of data representing background concentrations. A digital filtering technique using the fast Fourier transform and low-pass filters was used to smooth the selected data and to separate the seasonal cycle from the long-term increase in CO_2. The amplitude of the seasonal cycle was found to be increasing at a rate of 0.05 ± 0.02 ppm yr^{-1}. The average growth rate of CO_2 was 1.42 ± 0.02 ppm yr^{-1}, and the fraction of CO_2 remaining in the atmosphere from fossil fuel combustion was 59%. A comparison between the Mauna Loa continuous CO_2 data and the CO_2 flask sample data from the sea level site at Cape Kumukahi, Hawaii, showed that the amplitude of the seasonal cycle at Cape Kumukahi was 23% larger than at Mauna Loa, with the phase of the cycle at Mauna Loa lagging the cycle at Cape Kumukahi by about 1-2 weeks.

1. INTRODUCTION

The Mauna Loa Observatory (MLO), located at 19.5°N, 155.6°W on the island of Hawaii, is one of four baseline atmospheric monitoring stations operated by the Geophysical Monitoring for Climatic Change (GMCC) program of the National Oceanic and Atmospheric Administration (NOAA). The other three observatories are located at Barrow, Alaska; American Samoa; and South Pole Station, Antarctica. Continuous measurements of atmospheric CO_2 concentration have been made at Mauna Loa since 1958 by the Scripps Institution of Oceanography (SIO) [*Pales and Keeling*, 1965; *Keeling et al.*, 1976, 1982]. The long record of atmospheric CO_2 measurements at Mauna Loa is one of the most important data records for studies of the global carbon cycle and CO_2-induced climatic change.

Beginning in May 1974, GMCC has also made continuous measurements of atmospheric CO_2 at Mauna Loa independently of SIO, except for the calibration of CO_2 reference gases by SIO. The experimental methods used by GMCC for measuring CO_2 at Mauna Loa are described by *Komhyr* and *Harris* [1977] and *Komhyr et al.* [this issue]. A preliminary analysis of the data was given by *Peterson et al.* [1977]. Detailed descriptions of the observatory site are given by *Pales and Keeling* [1965], *Keeling et al.* [1976], and *Miller* [1978]. This study examines the GMCC measurements through the end of 1985.

Continuous measurements of CO_2 provide great detail for the study of CO_2 variability and its sources and sinks. We will first examine the variability in CO_2 concentration that occurs in 1 day or less, so that selection of the hourly average data representative of background conditions is possible. From these selected data we can then compute daily averages that are not influenced by local sources and sinks of CO_2. A linear digital filter is applied to these daily averages in order to extract the seasonal cycle and long-term trend information from the data. We have compared our results with those obtained from CO_2 measurements of flask samples taken at Cape Kumukahi, Hawaii, and have found significant differences in the amplitude and phase of the seasonal cycle at these two sites.

Paper number 89JD00315.
0148-0227/89/89JD-00315$05.00

2. CO_2 VARIABILITY

The concentration of atmospheric CO_2 observed at Mauna Loa varies on time scales ranging from less than 1 hour to annual and interannual cycles. In this section we will focus on the CO_2 variability that occurs over 1 day or less, so that we can select CO_2 values which we think are representative of a well-mixed air mass at Mauna Loa. Finding these "baseline" conditions is necessary so that the analysis of longer-period variations of CO_2 will not be affected by local sources and sinks of CO_2. We will begin by looking at the variability of CO_2 over very short (1 hour) time periods.

The magnitude of the variation of CO_2 during 1 hour can be obtained from the Control and Monitoring System (CAMS) data acquisition unit installed at Mauna Loa in November of 1984 [*Herbert et al.*, 1986]. For each hour this device reports the standard deviation of the 1-min average CO_2 analyzer voltages about the hourly average voltage. The standard deviation is then multiplied by a factor which depends on the sensitivity of the CO_2 analyzer for that hour, giving the hourly CO_2 variability in parts per million (ppm) of CO_2.

Figure 1 shows the distribution of the hourly CO_2 variability for all hours of 1985 that did not have any instrument malfunctions. Approximately 76% of the hourly CO_2 averages have standard deviations of less than 0.30 ppm. Also plotted in Figure 1 are the distributions of the hourly variability for 2 hours of the day, 0400 and 1400 LT. These hours are representative of the downslope (nighttime) and upslope (daytime) wind regimes that frequently occur at Mauna Loa [*Mendonca*, 1969].

At night, radiative cooling of the mountain causes a thin layer of cool, dry air to flow down the slopes of the mountain to the observatory. These downslope winds generally bring air

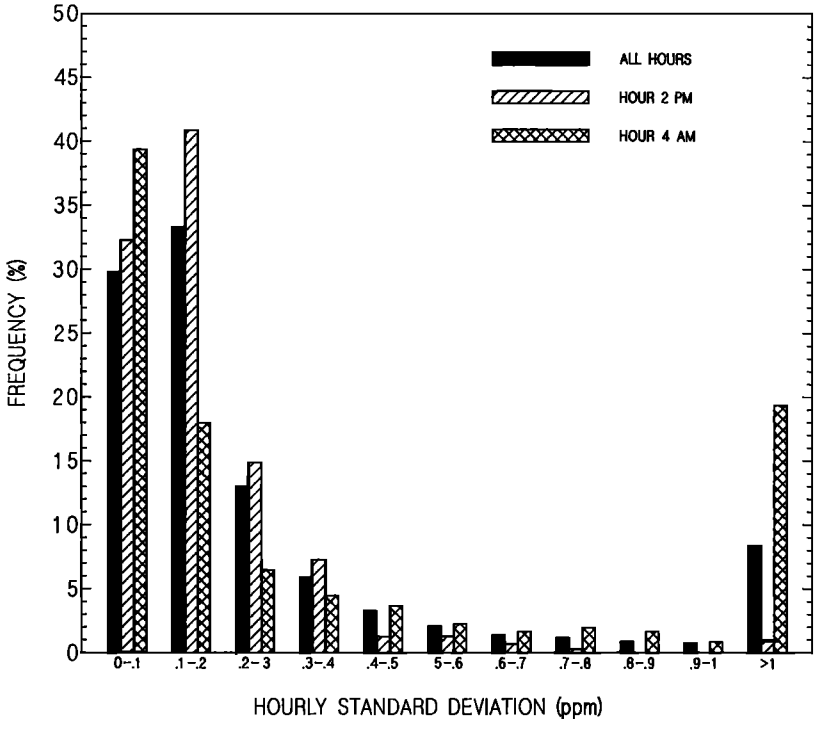

Fig. 1. Distribution of hourly CO_2 variability for 1985. The "hour 2 PM" bar is the distribution during typical afternoon upslope conditions, and the "hour 4 AM" bar is for typical nighttime downslope conditions.

with stable CO_2 concentrations (hourly variability <0.3 ppm), but they can also bring air with highly variable CO_2 concentration. This variability is due to air contaminated by outgassing of the Mauna Loa volcano [*Miller and Chin*, 1979]. Because of the proximity of the summit caldera to the observatory (~7 km), there is little mixing of the air before it reaches the observatory. As a result, nighttime hours tend to have either very steady CO_2 values or very variable CO_2 values. After the eruption of the Mauna Loa volcano in March of 1984, the number of hours during which volcanic contamination occurred increased dramatically (Figure 2). Even so, data representing "baseline" conditions are still present.

In contrast, daytime warming of the mountain causes upslope winds during the afternoon, bringing warm moist air to the observatory from the vegetated lower slopes of the mountain. This air tends to have CO_2 concentrations of low variability, usually less than 0.5 ppm. The steadiness of the afternoon CO_2 concentrations within an hour is a result of the large thickness of the air mass (up to 600 m) during upslope conditions and the distance between the observatory and the nearest vegetation that could affect CO_2 concentrations (~20 km). Thus the signal from local sources and sinks is thoroughly mixed into a deep layer of air by the time it reaches the observatory.

In addition to having low hourly variability, air that is brought up the mountain by the afternoon upslope winds is often depleted in CO_2. This is caused by uptake of CO_2 by island vegetation on the lower slopes of Mauna Loa [*Pales and Keeling*, 1965; *Keeling et al.*, 1976]. This afternoon depletion varies in magnitude, depending on the time of the year, and is largest during the summer months (Figure 3). The values shown in Figure 3 were obtained by first computing the daily average concentration, using only data from midnight to 0700 LT, and omitting hours with variable CO_2 concentrations. Next, the departure of each individual hourly value from the daily average was computed, and these differences were averaged over 1 month for each hour of the day.

The larger amplitude of the diurnal cycle during the summer results from a combination of several factors. The vegetation on the lower slopes of the mountain may be more photosynthetically active during the summer with increased uptake of CO_2. Upslope winds reach the observatory more often in summer than in winter [*Mendonca*, 1969]. Also during the summer the concentration of CO_2 at sea level is lower than the concentration of CO_2 at the elevation of Mauna Loa. We will examine the effect that this vertical gradient in concentration has on the diurnal cycle later in this paper, when CO_2 measurements made at the sea level site at Cape Kumukahi, Hawaii, are compared with those made at Mauna Loa Observatory.

3. DATA SELECTION

The objective of selecting data is to identify those hourly CO_2 values that are representative of well-mixed air at the latitude of Mauna Loa and which are not affected by some known local phenomenon. Although data selection can be based on independently measured parameters, such as wind speed and direction, we have used a statistical approach for rejecting certain data. The basic assumption is that the concentration of CO_2 in well-mixed air should change by only a small amount over several hours. This assumption is based on the fact that at very remote monitoring sites, such as South Pole, Antarctica, the variability within an hour and hour to hour is very small (<0.1 ppm, *Gillette et al.* [1987]). Although Mauna Loa is not as remote as the south pole, we should still use steady concentration values of CO_2 as an indicator of background air. Therefore for an initial selection process we

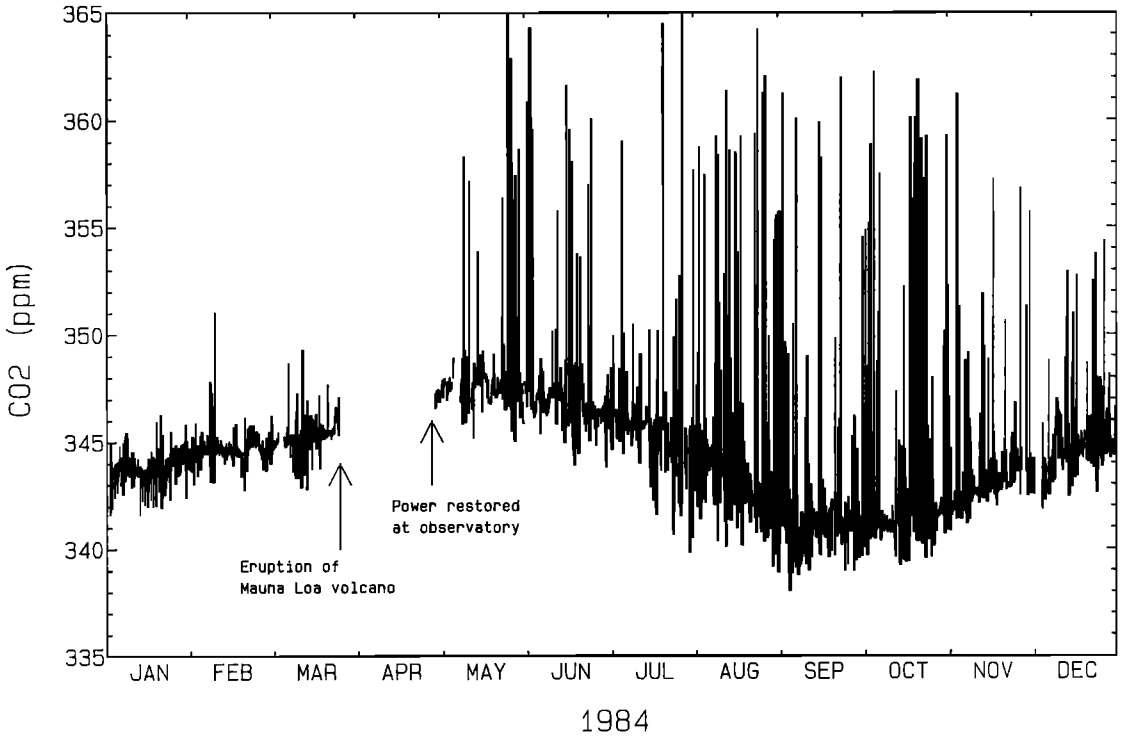

Fig. 2. Hourly average CO_2 concentrations for 1984. Power to the observatory was cut by lava flows from the Mauna Loa volcano in late March. Increased variability of CO_2 concentrations is evident after power was restored 1 month later.

have rejected data based on two criteria: instability of the CO_2 concentration within 1 hour and large changes in the CO_2 concentration from one hour to the next.

The first step in our data selection scheme is a comparison of the digitally recorded hourly average CO_2 concentrations with an analog recording of the CO_2 analyzer output on a strip chart recorder. Any hours that have significantly more variability in the air trace than in the reference gas traces are flagged. Because the decision about the variability in the chart traces is a subjective one, the actual minimum magnitude of the variability at which an hourly value is flagged can vary, but it is most likely in the range of 0.2-0.6 ppm for the standard deviation of minute averages about the hourly mean. We call the data record after this selection process our preliminary selected data set.

The second step is to remove hours where the concentration changed by more than a specified amount from 1 hour to the next. *Peterson et al.* [1982, 1986] stipulated that if the difference between consecutive hourly average concentrations was larger than 0.25 ppm, then both of those hourly values should be rejected. We have used a slight modification of this scheme in our selection process. Beginning with the preliminary selected data set, we calculated the hour-to-hour changes in CO_2 concentration and retained any two consecutive hourly values where the hour-to-hour difference was less than 0.25 ppm.

Although the two selection processes described (within an hour variability and hour-to-hour variability) removed much of the obviously variable data, visual inspection of the remaining data showed that most of the diurnal signal was still present, as well as groups of hourly values that stood out from the bulk of the remaining data. Since the diurnal cycle is clearly a local phenomenon, the hourly values affected by the afternoon drawdown in CO_2 concentration should not be included with the "baseline" data set. One way to exclude this data would be to use only nighttime (midnight to 0700 LT) CO_2 values. However, volcanic episodes that occur during the night can leave relatively few hours of data for analysis. In addition, uniform elimination of two-thirds of the data will remove valid measurements, since local influences on the daytime data are not observed all of the time. In order to alleviate these problems, an algorithm was developed for objectively removing data exhibiting afternoon diurnal variations and for removing any outliers that remain for the other times of the day.

The method for this final selection was to use an iterative approach, working with 1 month of hourly data at a time. First, those hours when the diurnal drawdown usually occurred (1100-1900 LT) were temporarily removed. Daily averages and corresponding standard deviations were calculated from the remaining hourly data, and a weighted spline curve [*Reinsch*, 1967] was fit to the daily averages. Then, for each day, those hourly concentrations which differed from the curve by more than twice the standard deviation for that day were removed. The process of calculating daily averages, fitting the spline curve, and removing hourly values was repeated until the standard deviation for each day was less than 0.3 ppm. At this point, those afternoon hours temporarily removed at the beginning of the selection that were within 0.3 ppm of the spline were replaced, as well as any hourly values which were removed in the previous step but were now within 0.3 ppm of the spline. The iterations were continued until no hourly values were removed or added.

The computer program never failed to converge and usually took about eight to ten iterations before finishing. Monthly and

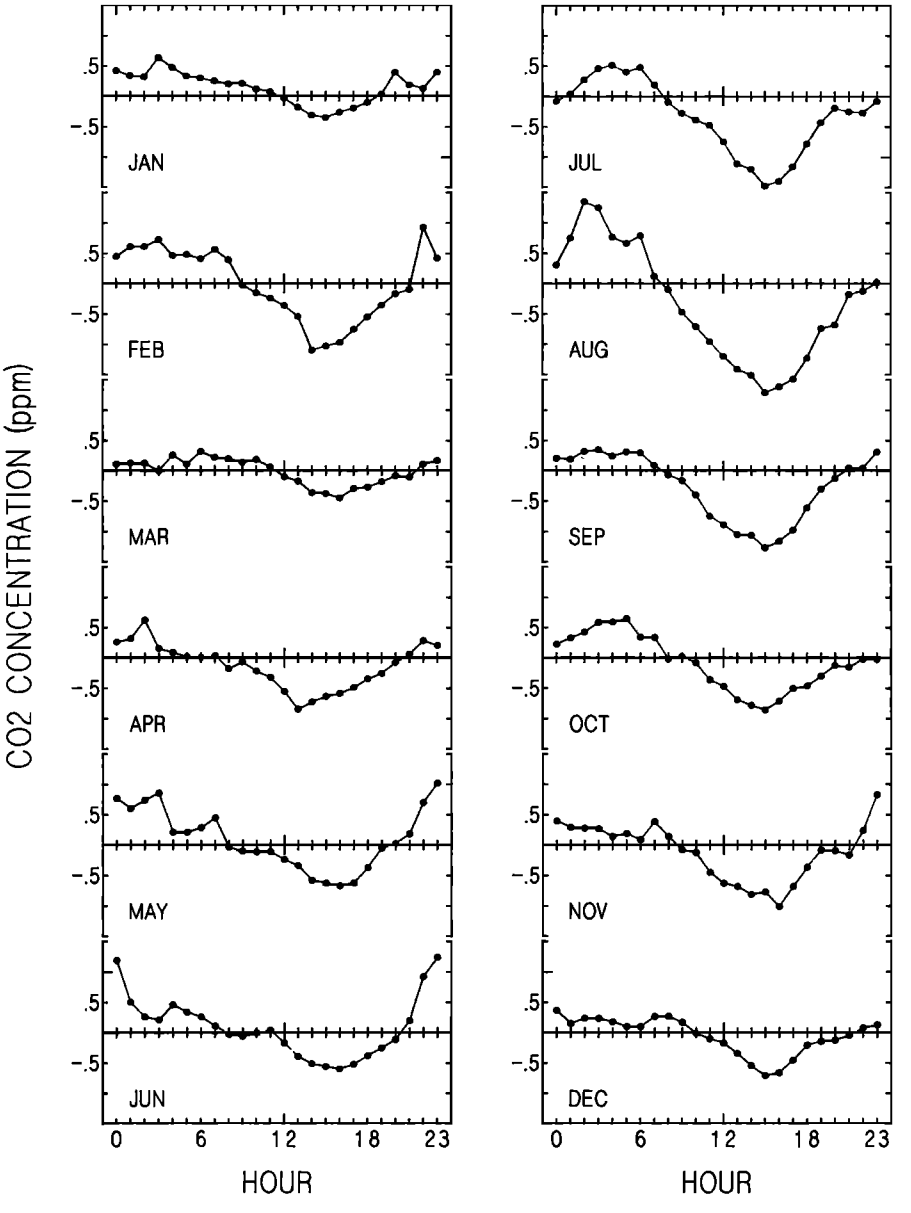

Fig. 3. Average amplitude for the diurnal cycle as a function of month. Values show the average departure from nighttime concentrations, omitting periods of high CO_2 variability.

annual means calculated from the final selected data are listed in Table 1. (The values under the column labeled "Data" are also shown by *Komhyr et al.* [this issue].) The selected daily averages for 1974 to 1985 are shown in Figures 4*a*-4*c*.

To compare different selection methods, three other selected data sets (in addition to the preliminary and final data sets) were created from the 1985 data. The first data set used nighttime hours (midnight to 0700 LT) and selected only those hourly averages for which the standard deviation for the hour was less than 0.30 ppm. The preliminary selection flags were ignored. This eliminates the problem of subjectivity and inconsistency in the selection of steady hourly values. However, the hourly standard deviation values are easily available only since November of 1984, so this method cannot be applied to the entire record. The second method used only the nighttime hours from the preliminary selected data set. In the third method, a 24-hour moving median through the data was used, and hourly values that were greater than 0.30 ppm from the median were rejected. This scheme is based on the assumption that the majority of data, or at least the middle values, over a 24-hour period (ignoring gaps in the data) represent baseline conditions, so that the median value will always be a background value. This method ignored the preliminary flagging of individual hours.

The results of this comparison of the five selection methods for 1985 are shown in Table 2, where the original data (without selection) have also been included. Figure 5 shows the result of each selection scheme for the months of January and August. Table 2 and Figure 5 show that generally all selection schemes arrived at the same result within a few tenths of a part per million, but that small systematic effects are present. The largest difference in the schemes is in the number of hourly values that remain. The monthly and annual averages calculated from the preliminary selected data set (which does

TABLE 1. Monthly and Annual Means Calculated From Final Selected Data

	1974				1975				1976			
	Data	N	σ_d	Filtered	Data	N	σ_d	Filtered	Data	N	σ_d	Filtered
Jan.				329.55	330.69	30	0.49	330.65	331.65	24	0.29	331.62
Feb.				330.79	331.41	28	0.42	331.45	332.66	28	0.55	332.47
March				331.90	331.84	24	0.27	331.93	333.53	26	0.87	333.56
April				332.98	333.26	29	0.47	333.23	334.80	24	0.48	334.71
May	333.15	15	0.31	333.19	333.92	30	0.35	333.81	334.80	31	0.59	334.77
June	332.07	27	0.37	332.20	333.39	28	0.44	333.38	334.14	24	0.34	334.14
July	330.99	31	0.48	330.97	331.81	25	0.81	331.76	332.88	20	0.59	332.94
Aug.	329.17	31	0.65	329.19	329.90	30	0.98	330.01	330.64	31	0.86	330.71
Sept.	327.39	29	0.54	327.38	328.56	29	0.72	328.44	329.01	25	0.91	329.00
Oct.	327.25	28	0.26	327.25	328.45	17	0.33	328.31	328.62	27	0.47	328.59
Nov.	328.26	28	0.35	328.25	329.29	25	0.42	329.37	330.13	26	0.43	330.05
Dec.	329.51	31	0.46	329.50				330.66	331.63	24	0.56	331.54
Annual	329.72			330.26	331.14			331.08	332.04			332.01

	1977				1978				1979			
	Data	N	σ_d	Filtered	Data	N	σ_d	Filtered	Data	N	σ_d	Filtered
Jan.	332.74	28	0.39	332.74	334.74	25	0.30	334.69	336.20	30	0.86	336.18
Feb.	333.23	27	0.38	333.32	335.22	26	0.44	335.21	336.65	26	0.24	336.80
March	334.91	29	0.52	334.83	336.52	30	0.62	336.52	337.79	26	0.76	337.73
April	336.01	28	0.34	336.02	337.77	28	0.36	337.79	338.95	23	0.46	338.82
May	336.82	29	0.21	336.76	338.00	30	0.37	338.03	339.03	20	0.63	339.20
June	336.13	26	0.32	336.13	338.04	27	0.40	337.95	339.22	29	0.47	339.17
July	334.75	28	0.52	334.76	336.39	29	0.62	336.35	337.58	28	0.75	337.66
Aug.	332.53	28	0.56	332.56	334.33	31	0.66	334.35	335.51	27	1.02	335.51
Sept.	331.27	24	0.47	331.23	332.35	19	0.77	332.41	333.83	26	0.64	333.80
Oct.	331.21	28	0.28	331.19	332.33	30	0.43	332.41	334.05	28	0.27	333.99
Nov.	332.36	28	0.37	332.33	333.77	28	0.34	333.74	335.26	30	0.55	335.27
Dec.	333.47	31	0.48	333.52	334.80	30	0.36	334.75	336.70	24	0.39	336.83
Annual	333.79			333.78	335.35			335.35	336.73			336.75

	1980				1981				1982			
	Data	N	σ_d	Filtered	Data	N	σ_d	Filtered	Data	N	σ_d	Filtered
Jan.	337.81	30	0.44	337.75	339.35	31	0.44	339.35	340.93	30	0.45	340.93
Feb.	338.26	26	0.47	338.35	340.47	27	0.76	340.41	341.67	26	0.44	341.71
March	340.07	31	0.66	339.92	341.73	28	0.64	341.71	342.78	30	0.36	342.73
April	340.87	30	0.30	340.97	342.47	28	0.32	342.58	343.71	30	0.49	343.63
May	341.48	31	0.33	341.48	343.02	31	0.12	342.95	344.31	31	0.36	344.30
June	341.30	30	0.55	341.26	342.46	28	0.41	342.43	343.41	29	0.38	343.45
July	339.36	25	0.72	339.23	340.78	29	0.52	340.80	341.96	30	0.56	341.91
Aug.	337.84	22	0.75	337.86	338.61	28	0.73	338.57	339.79	27	0.95	339.83
Sept.	335.98	25	0.63	336.11	337.04	26	0.53	336.97	337.91	25	0.86	337.92
Oct.	336.07	29	0.38	336.06	337.13	31	0.58	337.12	338.10	30	0.74	337.97
Nov.	337.22	27	0.36	337.20	338.49	29	0.54	338.55	339.27	26	0.69	339.30
Dec.	338.33	27	0.38	338.28	339.85	28	0.38	339.83	340.67	30	0.56	340.68
Annual	338.72			338.28	340.12			340.10	341.21			341.19

	1983				1984				1985			
	Data	N	σ_d	Filtered	Data	N	σ_d	Filtered	Data	N	σ_d	Filtered
Jan.	341.45	30	0.41	341.51	343.92	31	0.31	343.96	345.03	29	0.27	345.09
Feb.	342.69	27	0.42	342.43	344.64	29	0.23	344.61	345.89	25	0.41	345.86
March	343.42	29	1.23	343.52	345.18	23	0.30	345.32	347.47	27	0.57	347.39
April	345.17	25	0.55	345.09	347.10	2	0.14	346.50	348.02	25	0.48	348.08
May	345.79	29	0.40	345.81	347.45	25	0.39	347.34	348.73	31	0.52	348.74
June	345.40	25	0.54	345.43	346.80	23	0.42	346.83	348.11	29	0.55	348.05
July	343.99	28	0.92	343.90	345.44	28	0.65	345.42	346.59	27	0.51	346.56
Aug.	342.0	25	0.81	341.97	343.24	20	1.13	343.09	344.59	27	0.76	344.68
Sept.	340.02	27	0.62	340.04	341.25	24	0.77	341.24	343.01	27	0.86	343.03
Oct.	340.16	30	0.33	340.25	341.49	23	0.38	341.52	342.88	27	0.51	342.77
Nov.	341.39	29	0.44	341.37	342.84	27	0.62	342.85	344.19	28	0.66	344.22
Dec.	343.01	26	0.59	342.93	344.37	27	0.54	344.34	345.64	28	0.66	345.62
Annual	342.87			342.86	344.48			344.42	345.85			345.84

Columns labeled Data and σ_d contain the monthly means and sample standard deviations calculated directly from the selected daily averages. N is the number of data points. Column labeled Filtered contains the monthly means computed from daily values of the filtered data (see text). Annual means for the selected data are computed from monthly means. The annual means for the filtered data are computed from daily values.

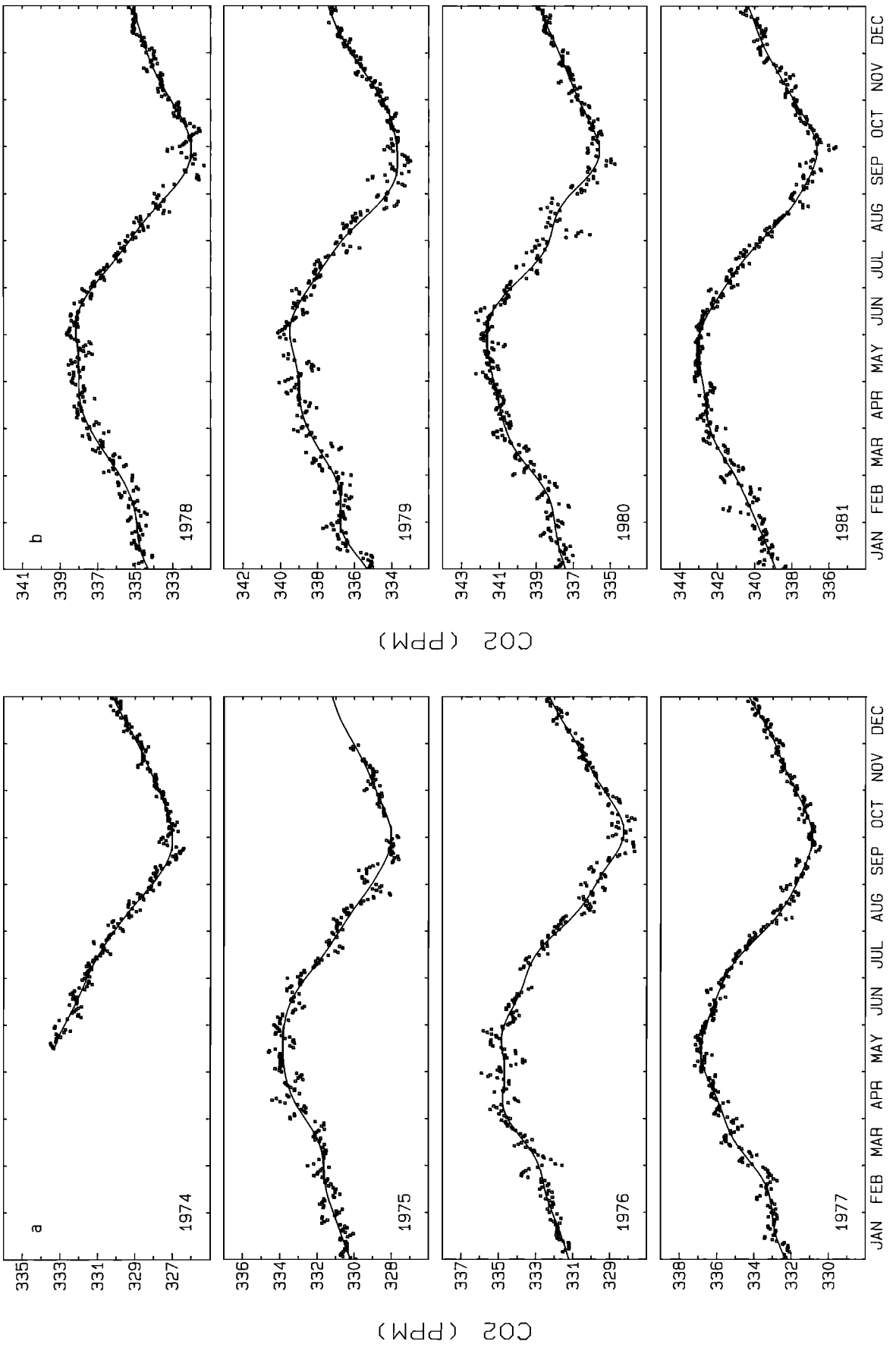

Fig. 4. Selected daily averages of CO_2 at Mauna Loa. The smooth curve is a computed by filtering the daily averages with a low-pass filter (see text). (*a*) 1974-1977; (*b*) 1978-1981; (*c*) 1982-1985.

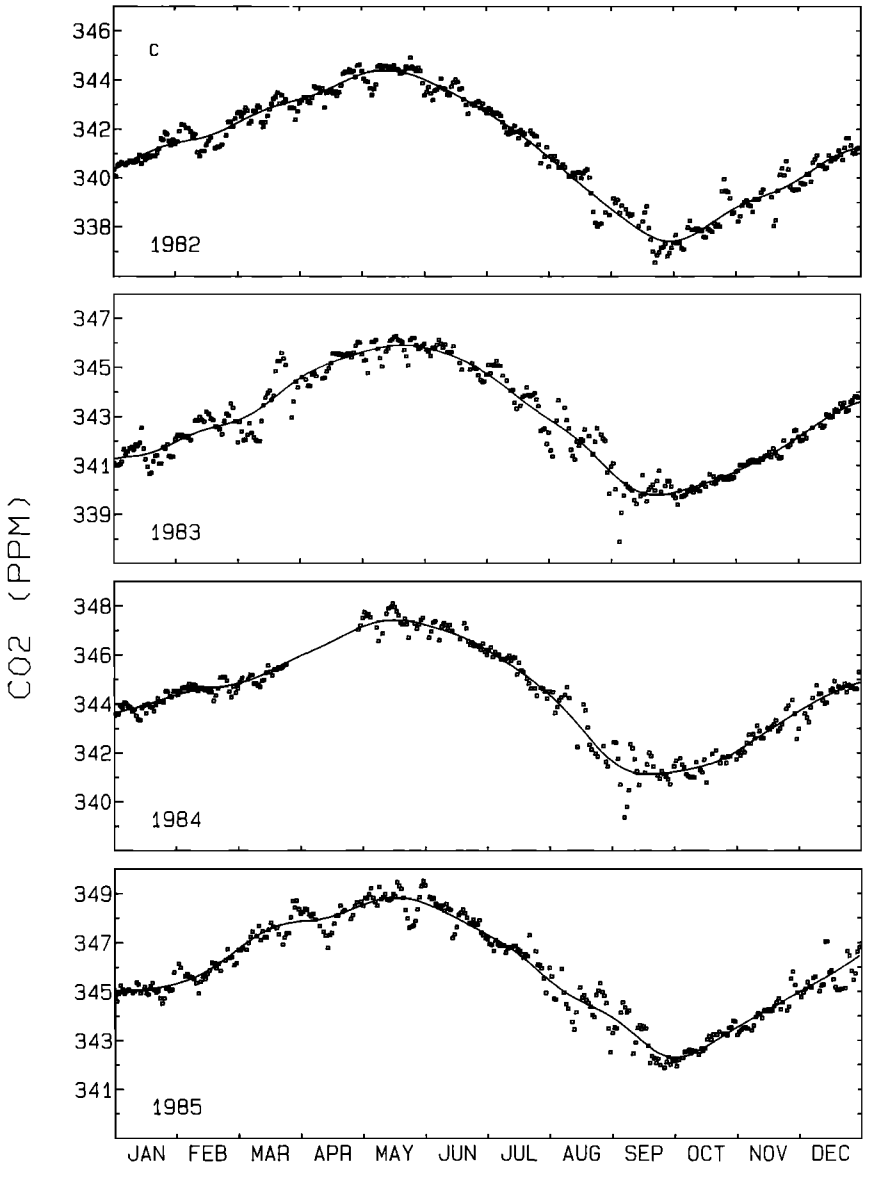

Fig. 4. (continued)

not include the hour-to-hour difference selection) are lower than the values from any of the other selected data sets because they include the afternoon drawdown in CO_2. The nighttime selection schemes (methods 3 and 4, Table 2) tended to yield values higher than the other selection methods, probably because they were not completely effective at removing high CO_2 values due to volcanic contamination. The assumptions for the running median selection method were probably violated for August. This could explain the low value observed when the running median tended to follow the strong afternoon drawdown during the middle of the month. We feel our final selection scheme is a good compromise for removing the diurnal cycle without sacrificing a large amount of the data.

4. Data Analysis

The record of CO_2 at Mauna Loa is basically a combination of three signals; a long-term trend, a nonsinusoidal yearly cycle, and short-term variations from several days to several weeks that are due to local and regional influences on the CO_2 concentration. Inspection of the daily averages in Figure 4 shows that these short-term variations occur frequently throughout each year, with magnitudes up to several parts per million. Once the data have been selected for background conditions, we need to apply additional filtering to remove these variations in order to investigate phenomena that occur over time scales longer than a few weeks. Our objective is to remove the short-term fluctuations from the record, then separate the long-term trend and annual cycle portions.

Several methods have been used by different investigators for filtering CO_2 data. The most common methods have been to fit a function to the data, such as an exponential trend with a series of harmonic terms [*Keeling et al.*, 1976; *Bacastow et al.*, 1985] or to use different types of splines [*Komhyr et al*, 1985; *Conway et al.*, 1988; *Wong et al.*, 1984]. Techniques involving complex demodulation and low-pass filtering [*Thompson et al.*,

TABLE 2. Comparison of Selection Methods for Mauna Loa, 1985

	Method*					
	1	2	3	4	5	6
Jan.	45.38	45.04	45.10	45.21	45.11	45.03
Feb.	46.28	45.70	46.13	46.08	45.88	45.89
March	47.70	47.33	47.43	47.42	47.49	47.47
April	48.36	47.83	48.02	48.18	48.04	48.02
May	49.12	48.66	48.92	48.94	48.83	48.73
June	48.57	47.97	48.18	48.25	48.15	48.11
July	46.60	46.04	46.71	46.67	46.54	46.59
Aug.	44.63	43.95	44.80	44.91	44.36	44.59
Sept.	43.02	42.70	43.14	43.17	42.98	43.01
Oct.	43.19	42.69	43.02	43.09	42.88	42.88
Nov.	44.30	44.12	44.33	44.33	44.17	44.19
Dec.	45.66	45.47	45.67	45.69	45.57	45.64
Number of hours	8227	6346	1619	1626	4201	3838
Annual	46.07	45.62	45.95	46.00	45.83	45.84

Values in parts per million above 300.00. Monthly averages are calculated using daily averages. Annual averages are calculated using monthly averages.

*Methods are as follows: 1, Complete data set (no selection); 2, preliminary selected data set; 3, preliminary selected data set for nighttime hours (midnight to 0700 only); 4, nighttime hours (midnight to 0700) where hourly standard deviation is less than 0.3 ppm; 5, selected using 24-hour running median; 6, final selected data set.

1986] and digital filtering [*Cleveland et al.*, 1983; *Enting*, 1987] have also been used. Our method for filtering uses the fast Fourier transform (FFT) algorithm to convert the data set from the time domain into the frequency domain, apply a low-pass filter in the frequency domain to separate the features of interest, then perform an inverse FFT to convert the filtered data back into the time domain.

4.1. *Fourier Transform*

The FFT algorithm requires that the data be equally spaced in time and without any gaps. Since we are using daily values for the analysis, we first filled any gaps longer than about 7 days with daily CO_2 values from the SIO continuous analyzer at Mauna Loa [*Keeling et al.*, 1986]. Because measurements by GMCC did not begin until May 1974, selected SIO daily values at 5-day intervals from January 1 to May 16, 1974, were used to obtain a complete year for 1974. Breaks that occurred when data from both continuous analyzers were missing were partially filled by using daily CO_2 values from the GMCC CO_2 flask sampling program [*Komhyr et al.*, 1985; *Conway et al.*, 1988]. All remaining gaps were filled by linear interpolation. A total of 4382 points were used, of which 86.1% were GMCC daily averages, 1.9% were SIO daily averages, 0.3% were flask values, and 11.8% were interpolated.

The FFT also requires that the number of points used be an integral power of 2. Therefore the data must be "zero padded" to obtain the required number of points. This is done by first removing from the data the mean and a linear trend which passes through the first and last data points, so that the data set is approximately centered around zero and begins and ends with zero. The data record is then extended by 1 or 2 years (depending on the type of filtering, explained later) on each end by repeating the first and last years of data, with the provision that the added data begin and end each year at zero. This extrapolation was included to minimize any end effects that occurred during the filtering process. An equal number of points with zero value are then added at each end of the data until the required number of points is obtained.

The data set is then converted into the frequency domain using the fast Fourier transform algorithm. The transformed data is multiplied by a low-pass filter function (see later discussion) which retains only the desired frequencies in the data. An inverse FFT is calculated to convert the data back to the time domain. The mean and linear trend removed previously are then added back into the data to arrive at the final filtered data set.

4.2. *Power Spectrum*

The power spectrum of the Mauna Loa record is shown in Figure 6. The spectrum was computed by smoothing the (10% tapered) periodogram with two passes of a modified Daniell filter [*Bloomfield*, 1976]. The spectrum in the insert is for the low-frequency portion of the spectrum in which the annual cycle and its harmonics are situated. This portion has been smoothed to a lesser extent in order to retain the separation between the peaks in the harmonics. It is clear that the annual cycle fundamental and its first harmonic (6-month period) are significant (see, for example, *Keeling et al.* [1976]). In order to evaluate whether any other peaks in the spectrum are significant, we need a base for comparing the significance levels.

The Mauna Loa CO_2 record shows a large degree of "persistence," that is, each value is influenced by the immediately preceding value. Thus the power spectrum will have a different shape from that due to a purely random process. We can approximate the shape of a power spectrum that has persistence by computing the spectrum of a first-order autoregressive process and use this "null" continuum for determining if any nonrandomness is present in the power spectrum [*World Meteorological Organization*, 1966]. The shape of the "null" continuum depends on the value of the lag one auto covariance in the data. Before we computed this value though, we first needed to remove any influences caused by the

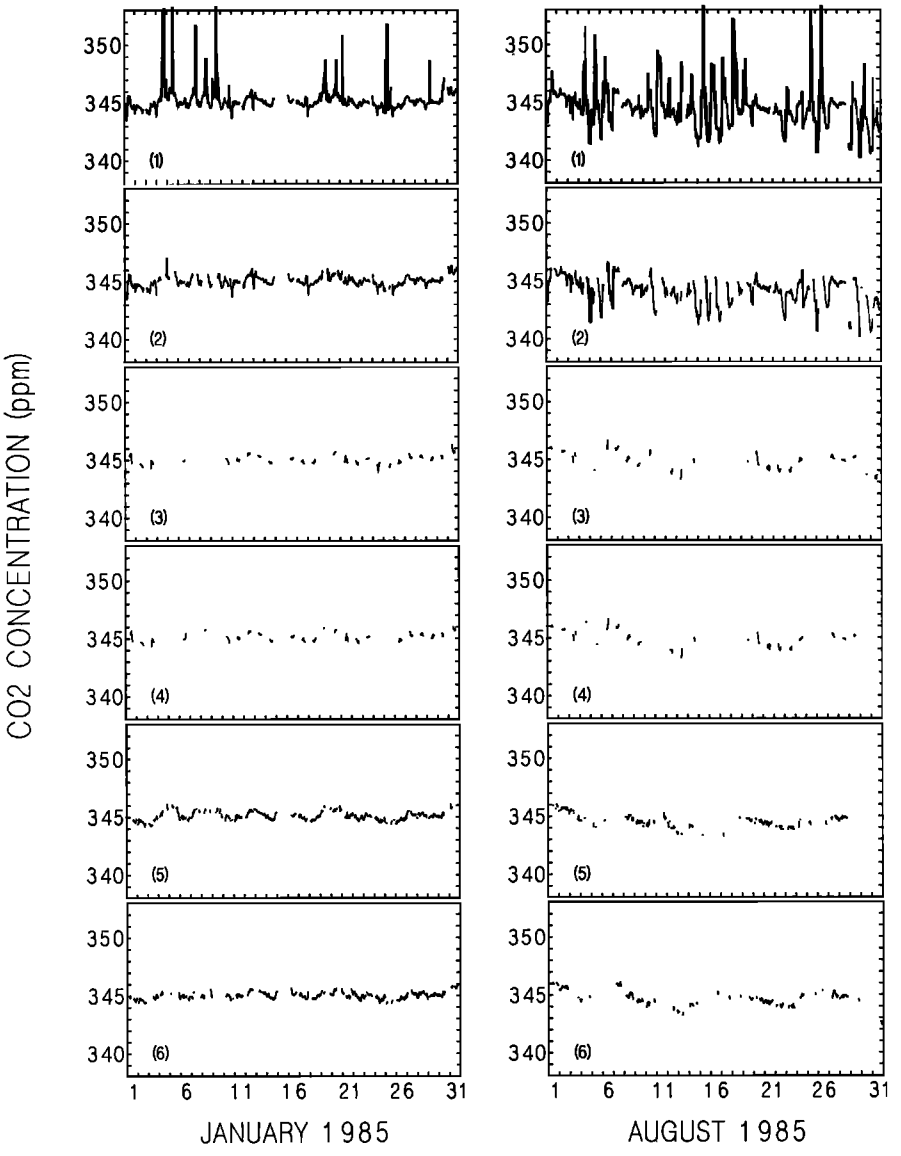

Fig. 5. Results of different selection schemes for typical winter and summer months. The plots correspond to the selection methods described in Table 2.

annual cycle fundamental and its first harmonic. To do this, we made a least squares fit of the detrended data to the function

$$x(t) = \sum_{i=1}^{2} A_i \cos(\omega_i t) + B_i \sin(\omega_i t) \quad (1)$$

using the methods described by *Bloomfield* [1976, chap. 2]. This function was then subtracted from the data. The lag one auto covariance was then computed, and the "null" spectrum was determined using this value. This spectrum is shown as the smooth solid curve in Figure 6, with the associated 5 and 95% confidence levels shown as the dashed curves.

A comparison of the Mauna Loa spectrum with the "null" continuum shows that the second harmonic of the annual cycle (3 cycles yr^{-1}) and higher harmonics are not significant. However, there is a band of frequencies with periods between 1 and 2 weeks that appears to be significant and accounts for the short-term events seen in Figures 4*a*-4*c*. These events occur over too long a period to be removed in the data selection process, which removes mainly local effects. Although *Sadler et al.* [1982] showed that there was little relationship between CO_2 variability at Mauna Loa and large-scale atmospheric circulation, specific events could probably be correlated with the arrival of distinct air masses at Mauna Loa. Several investigators examined this type of variability at the high northern latitude station at Barrow, Alaska [*Halter and Peterson*, 1981; *Halter and Harris*, 1983; *Halter et al.*, 1985] and were able to relate this variability to regional sources and sinks of CO_2 and to transport of anthropogenic CO_2 from other latitudes and regions.

4.3. *Data Filtering*

The short-term variations due to the high-frequency part of the spectrum can be removed by applying a low-pass filter with an appropriate cutoff frequency, which is defined as the frequency at which the filter attenuates the amplitudes of the cycles by one half. The transfer function of the filter we used is a decreasing exponential,

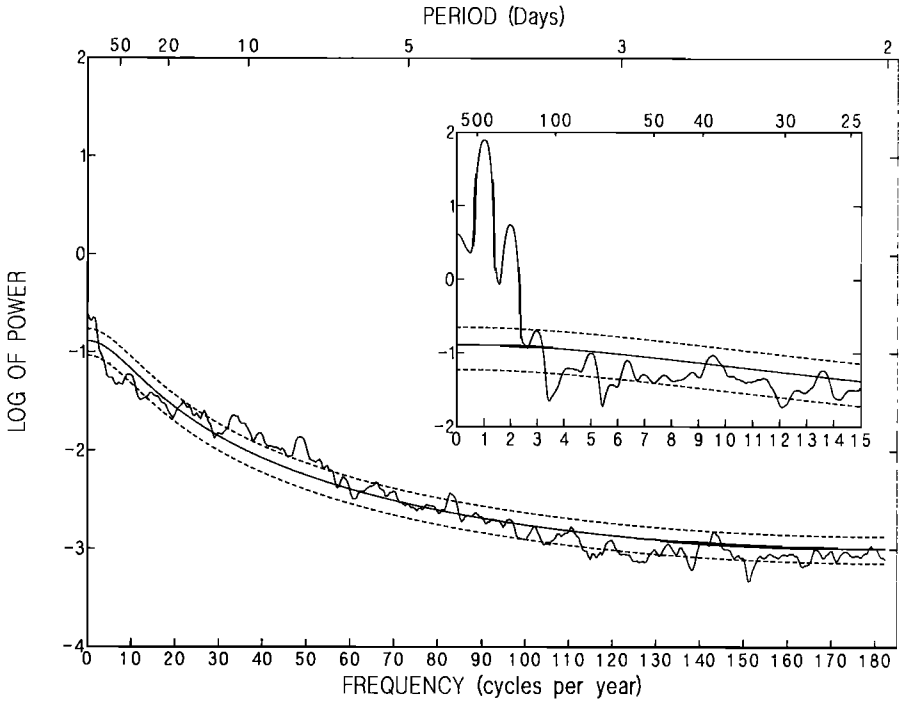

Fig. 6. Smoothed power spectrum of the Mauna Loa daily average data. The inset has been smoothed less in order to retain the separation between peaks. The smooth solid curve represents the power spectrum of a one-lag autocovariance function. The dashed curves are the 5% and 95% confidence levels.

$$H(f) = \exp\left[-c_1 \left(\frac{f}{f_c}\right)^p\right] \qquad (2)$$

where f_c is the cutoff frequency in cycles per day, c_1 is a normalizing coefficient set equal to ln(2) so that $H(f) = 0.5$ at $f = f_c$, and p is an integer which we set equal to 4.

Since uniform atmospheric mixing in the northern hemisphere occurs within 2-3 months [*Czeplak and Junge*, 1974] and if the Mauna Loa record is to represent the CO_2 cycle for a latitude zone, any frequencies higher than about 6 cycles yr^{-1} should be removed from the record and frequencies lower than this should be relatively unchanged. Thus for the removal of short-term variations in CO_2, we have chosen the cutoff point to be at cycles with periods of 50 days (f_c = 7.3 cycles yr^{-1}). For this cutoff value we extended the seasonal cycle for 1 year on each end of the data. A plot of the transfer function with the 50-day cutoff is shown as the solid curve in Figure 7*a*. The result of applying the filter with a 50-day cutoff is shown as the solid curve in Figure 8 and in Figures 4*a*-4*c*. The data record is much smoother after filtering owing to the removal of the high-frequency portion of the record. Monthly and annual means computed from the filtered data are shown in Table 1.

The long-term trend can be separated from the record by again applying a low-pass filter, but this time removing periods of 1 year and shorter. The long-term trend then consists of cycles with periods longer than 1 year in length. A cutoff frequency of about 0.55 cycles yr^{-1} (667-day period) was chosen, because with this cutoff point the value of the filter transfer function is almost zero at the frequency of the annual cycle fundamental. For this cutoff we extended the seasonal cycle by 2 years on each end of the data. The values of the filter transfer function with this cutoff are shown as the dashed curve in Figure 7*a*. The result of the filtering operation with a 667-day cutoff is shown as the dashed curve in Figure 8.

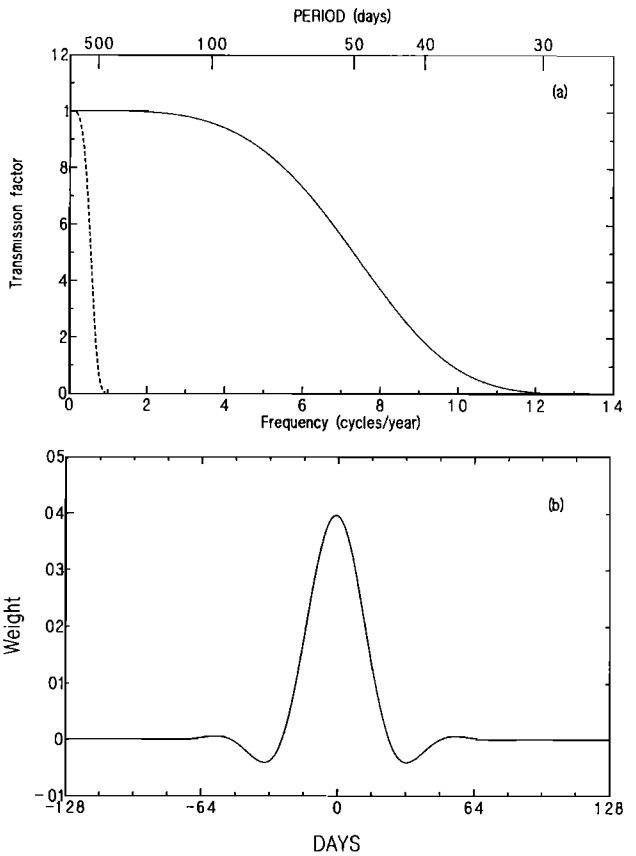

Fig. 7. (*a*) Frequency response functions of the exponential filter at cutoff points of 50 days (solid curve) and 667 days (dashed curve). (*b*) The inverse transform of the frequency response curve, representing the weights of the filtering function in the time domain. The exponential curve is shown by the solid curve at the 50-day cutoff point.

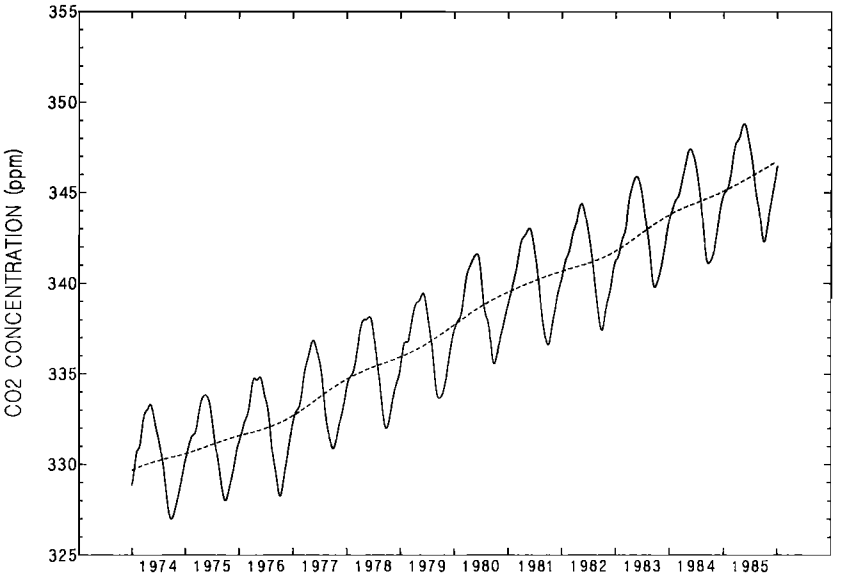

Fig. 8. Results of the filtering operations applied to the Mauna Loa daily averages. The solid curve is for a cutoff point at 50 days, and the dashed curve for a cutoff point at 667 days.

4.4. *Statistical Uncertainty of the Filter*

Filtering with this method in the frequency domain is functionally equivalent to convolution filtering in the time domain [*Koopmans*, 1974, pp. 180-182]. That is, filtering in the frequency domain can be visualized as a weighted moving average process in the time domain, which takes the form

$$x'(t) = \sum_{j=-n/2}^{+n/2} c_j x(t+j) \qquad (3)$$

where c_j are the filter weights and n is the number of weights. These weights are the values of the impulse response function (IRF) of the filter transfer function. The IRF is the inverse transform of the filter transfer function and is a measure of how the filter responds to a delta function impulse in the time domain. Figure 7*b* shows the IRF of the exponential filter for the cutoff point at 50 days. The number of weights specified at daily intervals in the time domain that are required to exactly reproduce the results obtained by filtering in the frequency domain is large and is approximately equal to the value of the cutoff period.

We can use this formulation of the filter in the time domain to facilitate estimation of the statistical uncertainty associated with the filtered time series. The theory of error propagation shows that the statistical uncertainty (variance) for each filtered value $x'(t)$ is

$$\sigma^2_{x'(t)} = \sum_{i=1}^{n} c_i^2 \sigma^2_{x(t)} + 2 \sum_{j=1}^{n-1} \sum_{k=j+1}^{n} c_j c_k \sigma^2_{x_j x_k} \qquad (4)$$

where $\sigma_{x(t)}$ is the uncertainty of the data point $x(t)$ prior to filtering. The second term in (4) is the covariance term, where $\sigma_{x_j x_k}$ is the covariance between the points x_j and x_k, and is included to account for the serial correlation in the data. If we make the assumption that the variances for each individual data point are equal and that the $\sigma^2_{x_j x_k}$ can be approximated by the lags in a first-order auto regressive process, $r(k) = r(1)^k$, $k = 1, 2, \cdots$, then (4) becomes

$$\sigma_s^2 = \sigma_{rsd}^2 \sum_{i=1}^{n} c_i^2 + 2 \sum_{j=1}^{n-1} \sum_{k=j+1}^{n} c_j c_k r_{k-j} \qquad (5)$$

The sum of the squares of the filter weights for the 50-day cutoff is 0.033. Rather than using the uncertainties for each data point to compute the uncertainty in the filtered data, we used instead the standard deviation of the residuals of the original data points about the filtered points as our estimate of the "noise" in the data and use this value of 0.38 ppm for σ_{rsd} in (5). The value for σ_s was calculated to be 0.11 ppm, which is the statistical uncertainty associated with any daily value in the filtered data. The sum of the squares of the filter weights for the 667-day cutoff is 0.0025. We have again used the value for σ_{rsd} of 0.38 ppm, which gives a statistical uncertainty σ_s of 0.03 ppm for the trend data.

The statistical uncertainty of the trend data is small enough that other errors, such as calibration and measurement errors, as well as uncertainties due to data selection become significant at this level. However, it is difficult to determine a precise value for these other, nonstatistical errors. We will take a conservative approach and assign the same uncertainty of 0.11 ppm for the trend data that was found for the 50-day-cutoff filter. Because the extrapolated data at the ends of the actual record will differ somewhat from the true values, there is a larger uncertainty for the first and last years of the trend. We have tried to estimate this uncertainty in an empirical manner, based on different extrapolation techniques and using different lengths of the record. The values of the trend at the ends tend to vary on the order of 0-0.2 ppm. We therefore assign an uncertainty of 0.2 ppm for the trend data of 1974 and 1985 and 0.11 ppm for the years in between.

4.5. *Seasonal Cycle*

It can be seen from Figure 8 that the annual cycle has the same basic shape from year to year, although with some small but significant variations. For example, the peaks of the cycles

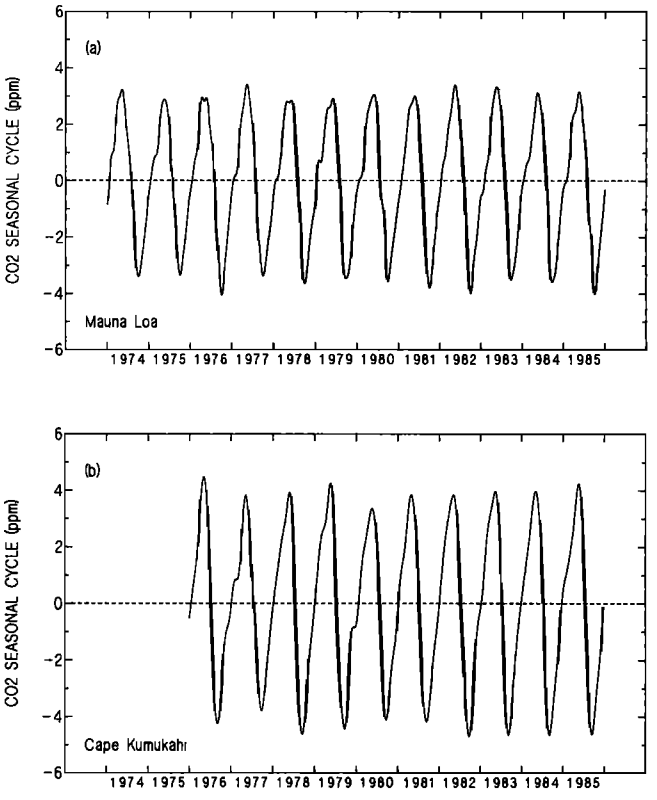

Fig. 9. Detrended seasonal cycle for (*a*) Mauna Loa and (*b*) Cape Kumukahi. The curves were obtained by subtracting the dashed curves in Figure 8 and Figure 13 from the solid curves in those same figures for Mauna Loa and Cape Kumukahi, respectively.

can vary from a sharp point to a more rounded shape. The "shoulder" during the CO_2 rise near the beginning of each year is sometimes missing or reduced in size, as in 1976 and 1981. By subtracting the trend values from the smoothed values of Figure 8, the detrended annual cycle remains, as is shown in Figure 9*a*. This assumes that the annual cycle is made up of the entire band of frequencies between 1 cycle yr^{-1} and the frequencies retained by the smoothing filter (7.3 cycles yr^{-1}), not just of the fundamental and harmonic frequencies. The characteristics of the Mauna Loa seasonal cycle are listed in Table 3. The peak of the cycle occurs in mid-May and the trough in late September or early October. The mean peak-to-peak amplitude for the 12 years from 1974 to 1985 was 6.77 ppm, with a standard deviation about the mean of 0.32 ppm.

Bacastow et al. [1985] reported a statistically significant increase in the amplitude of the Mauna Loa seasonal cycle, based on measurements from 1958 to 1982. *Pearman and Hyson* [1981] and *Cleveland et al.* [1983] also found a significant increase. Working with a much shorter record, we have also found a significant increase in the seasonal amplitude. A weighted least squares linear regression (*Program LINFIT* [*Bevington*, 1969]) was fitted to the amplitude values of Table 3. The statistical uncertainty for each individual amplitude value was calculated to be 0.22 ppm for 1975-1984 and 0.34 ppm for 1974 and 1985. The slope of the regression line was found to be 0.045 ± 0.021 ppm per year (Figure 10).

The amount of smoothing by the filter can affect the results obtained. To show this, we also calculated the seasonal amplitude characteristics using filter cutoff points at 80 days and at 20 days. The mean amplitude was found to be 6.65 ± 0.24 ppm and to be increasing at the rate of 0.039 ± 0.019 ppm yr^{-1} for the 80-day cutoff, and a mean amplitude of 7.16 ± 0.43 ppm with an increase of 0.033 ± 0.025 ppm yr^{-1} for the 20-day cutoff. The higher uncertainties for the 20-day cutoff are due to the inclusion of short-term variations in the data that are removed when using higher cutoff points.

Enting [1987] found a correlation between the peak heights for each spring and the following fall for SIO monthly mean data from 1960 to 1981. Low-amplitude peaks in the spring were followed by low-amplitude troughs in the following fall. He did not find any correlation between the fall troughs and the following spring peak. If we plot the absolute values of the maximum and minimum values for the seasonal cycle (Table 3) in a manner analagous to that of Enting, we find a correlation opposite to that stated by Enting. We see no correlation between the size of the peaks and troughs in the same year (correlation coefficient $r = 0$, Figure 11*a*), but we do find a correlation for the size of the fall troughs followed by the spring peak ($r = 0.86$, Figure 11*b*).

In an attempt to explain this difference, we also analyzed the SIO monthly mean data in the same manner that we analyzed the GMCC daily average data. We were nearly able to reproduce Enting's results using a filter with a low-frequency cutoff point (150 days), but the correlations changed when a higher-frequency cutoff was used. We also found that the later years of the record had a higher correlation between the fall trough and the following spring peak than the earlier years. The NOAA monthly mean data also gave slightly different correlation values than the SIO data. Thus these correlations seem to depend on the filtering technique, the averaging time of the data, and the period of data used. Enting's results may be due to significant autocorrelation in his digital filter for the time span between the maximum and minimum in the seasonal cycle (I. Enting and M. Manning, personal communication, 1988). This was found by passing the filter through white noise and calculating the autocorrelation at various lags. We computed the autocorrelation of our filter in the same manner and found it to be negligible for the time spans of interest (approximately 136 and 229 days).

The dates at which the minima of the annual cycle occur are more consistent than the dates of the maxima. The dates at which the seasonal cycle crosses the trend line are also more consistent for the drawdowns in July than for the increases in January. *Peterson et al.* [1986] found a similar consistency for the continuous CO_2 measurements at Barrow, Alaska. This suggests that the forces that drive the summer CO_2 drawdown in the northern hemisphere are stronger and more regular than any interannual variability in CO_2 but that during the winter and spring the release of CO_2 by the biosphere and atmospheric transport are more variable in time and more easily affected by regional or hemispheric variations in CO_2. This can also be seen in Figure 4, where there tend to be larger and more frequent excursions from the filtered curve during the first half of the year than in the latter half.

4.6. *CO_2 Growth Rate*

The trend line of Figure 8 is the result of fossil fuel combustion, changes in the amount of carbon held in standing biomass and soils, and global-scale phenomena such as El

TABLE 3. Seasonal Amplitude Characteristics of CO_2 at Mauna Loa

Year	Maximum	Max DOY	Minimum	DOY	Amplitude	Cross	
						+	−
1974	3.23	131	-3.41	276	6.64	20	211
1975	2.88	135	-3.36	277	6.24	16	207
1976	2.96	105	-4.06	281	7.02	17	212
1977	3.42	133	-3.39	277	6.81	15	210
1978	2.85	157	-3.67	272	6.52	20	211
1979	2.91	154	-3.48	271	6.39	12	212
1980	3.06	152	-3.59	274	6.65	19	203
1981	3.01	141	-3.82	273	6.83	25	207
1982	3.39	134	-4.00	275	7.39	10	209
1983	3.33	137	-3.52	267	6.85	32	212
1984	3.12	138	-3.60	265	6.72	11	213
1985	3.16	138	-4.03	275	7.19	25	208
Average	3.11	138	-3.66	274	6.77	19	210
s.d.	0.20	14	0.26	4	0.32	6	3

Maximum and minimum refer to largest deviation from trend line in parts per million. Amplitude indicates maximum minus minimum. Max DOY and Min DOY are dates of maximum and minimum in day of year. Cross plus and minus signs refer to the day of year where seasonal cycle crosses the trend line; s.d. is one standard deviation about the average.

Niño, which cause interannual variations in the CO_2 growth rate. We can determine the time variation of the CO_2 growth rate by computing the derivative of the trend line in Figure 8. The resulting curve is shown as the solid line in Figure 12, with an associated statistical uncertainty of 0.16 ppm yr^{-1}. The mean growth rate for 1974-1985 was 1.42 ppm yr^{-1}, with a standard error of the mean of 0.02 ppm yr^{-1}.

The upward slope of the trend line in Figure 8 is related to the global emissions of fossil fuel CO_2. For the Mauna Loa record from January 1, 1974 to January 1, 1985, the concentration of CO_2 increased by 15.41 ppm (Table 4). For these 11 years the total global input of CO_2 from fossil fuel and cement production was 55.62×10^{15} g of carbon [*Rotty, 1987*], which corresponds to 26.23 ppm of CO_2, based on a value of 5.12×10^{21} g for the dry mass of the atmosphere [*Trenberth*, 1981] and a mean molecular weight for the atmosphere of 28.97 g. Therefore the fraction of fossil fuel CO_2 that remained airborne during this period was 58.7%. This value is very close to the value of 56.9% given by *Keeling et al.* [1985] for the SIO Mauna Loa CO_2 record from 1959 to 1983 and to the value of 59.6% for the years 1970-1981 for the site at Station P in the North Pacific. *Peterson et al.* [1986] found a value of 53% for the Arctic site at Barrow, Alaska.

The airborne fractions computed for the individual years show a large amount of scatter (Table 4), ranging from about 42% in 1974 to 84% in 1983. The variations in fossil fuel emissions are too small too account for the range in airborne fraction values. Rather, the variability in airborne fraction is due to large interannual variations in the growth rate of CO_2. Figure 12 shows growth rate minima occurring in 1974, 1976, 1978, 1982, and 1984 (approximately every 2-3 years), with corresponding maxima 1 year later. These changes in growth rate have been found to correlate with the Southern Oscillation Index (SOI) [e.g., *Bacastow*, 1976,1977; *Bacastow et al.*, 1980; *Komhyr et al.*, 1985, *Conway et al.*, 1988]. We have computed the cross correlation coefficients between monthly averaged CO_2 growth rates and monthly averaged SOI values [*Climate Analysis Center*, 1986] shown in Figure 12 for several lag times of the SOI. The maximum correlation coefficient was found to be -0.56 ± 0.24 for a lag of 5 months. That is, the SOI minimum occurs approximately 5 months before the maximum in the CO_2 growth rate. The mechanism leading to this correlation is not clear, however. *Thompson et al.* [1986] found the variations in CO_2 growth rates to be correlated with several geophysical variables individually (SOI, wind stress, sea surface temperature), but once the SOI was included, additional parameters did not improve the correlations.

5. COMPARISON WITH CAPE KUMUKAHI

Since 1976, flask measurements of atmospheric CO_2 have been made at Cape Kumukahi on the eastern shore of the island of Hawaii as part of the NOAA GMCC flask CO_2 measurement

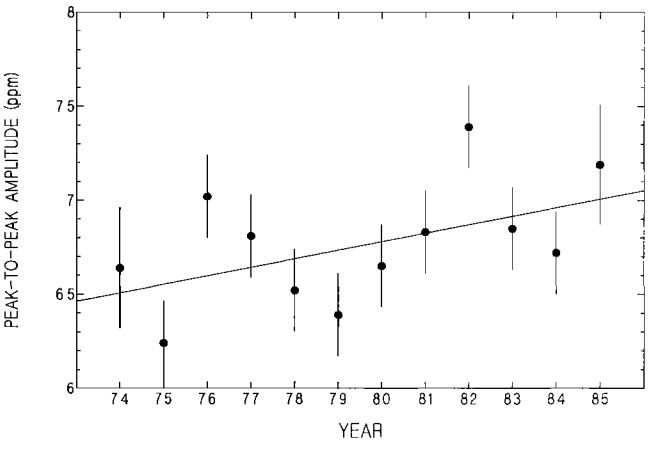

Fig. 10. Increase in the peak-to-peak seasonal amplitude for Mauna Loa. The straight line is from a weighted linear regression to the data. The error bars are the statistical uncertainty (one standard deviation) for each amplitude value.

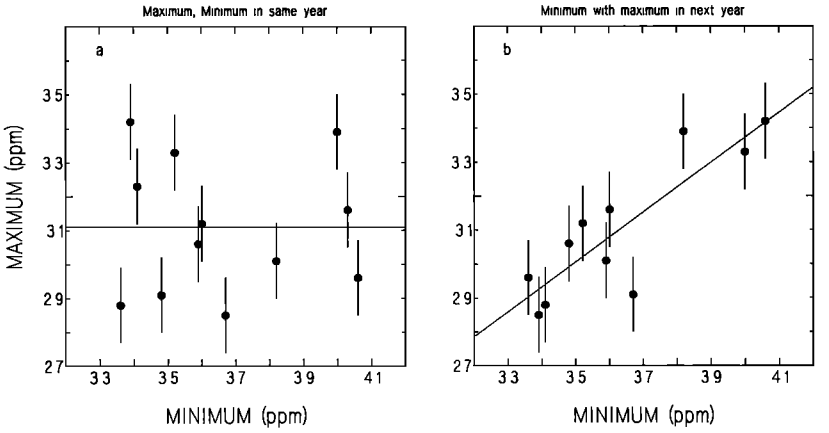

Fig. 11. Scatter plots of the maximum and minimum seasonal amplitude values listed in Table 3. (*a*) The maximum and minimum values in the same year. (*b*) The values for the minimum with the maximum in the following year.

program [*Komhyr et al.*, 1985; *Conway et al.*, 1988]. It is known that vertical gradients of CO_2 can occur in the lower atmosphere [*Bolin and Bischof*, 1970; *Bischof*, 1971; *Pearman and Beardsmore*, 1984; *Tanaka et al.*, 1987]. With an elevation difference of 3394 m between Mauna Loa and Cape Kumukahi, we can expect to see significant differences in the CO_2 signal between these sites.

Figure 13 shows the flask sampling record at Cape Kumukahi for all the years up to 1985. Sample collection, analysis, and data selection are explained by *Komhyr et al.* [1985] and *Conway et al.* [1988]. One or two pairs of flask samples are collected approximately once per week. After data selection the remaining data have been averaged to provide one value per sample day and are shown as the crosses in Figure 13. The Cape Kumukahi data are expressed in the same scale as the Mauna Loa analyzer data [see *Komhyr et al.*, this issue] and are therefore directly comparable with each other.

We have filtered the Cape Kumukahi data in a manner similar to that descibed above for the Mauna Loa data, except that the data points were at weekly rather than daily intervals. The greater time interval between weekly flask samples and daily averages from continuous data causes the power in the spectrum that is associated with frequencies between 0.5 cycles per week (the highest frequency possible for weekly flask sampling) and 0.5 cycles per day (the highest frequency when using daily averages) to be aliased into the lower-frequency part of the spectrum. Thus the Kumukahi data have a greater proportion of power in the low-frequency cycles than do the Mauna Loa data. Therefore we have used a frequency cutoff that removes the same proportion of power that was removed in the Mauna Loa data. A frequency cutoff point at 83 days (compared to 50 for Mauna Loa) was used for smoothing the Cape Kumukahi data. The result of filtering the Cape Kumukahi data is shown as the solid line in Figure 13. The statistical error associated with the filtered data was estimated to be 0.21 ppm. The trend was separated from the record in the same manner as for Mauna Loa and is shown as the dashed line in Figure 13. We have assigned the same uncertainty of 0.21

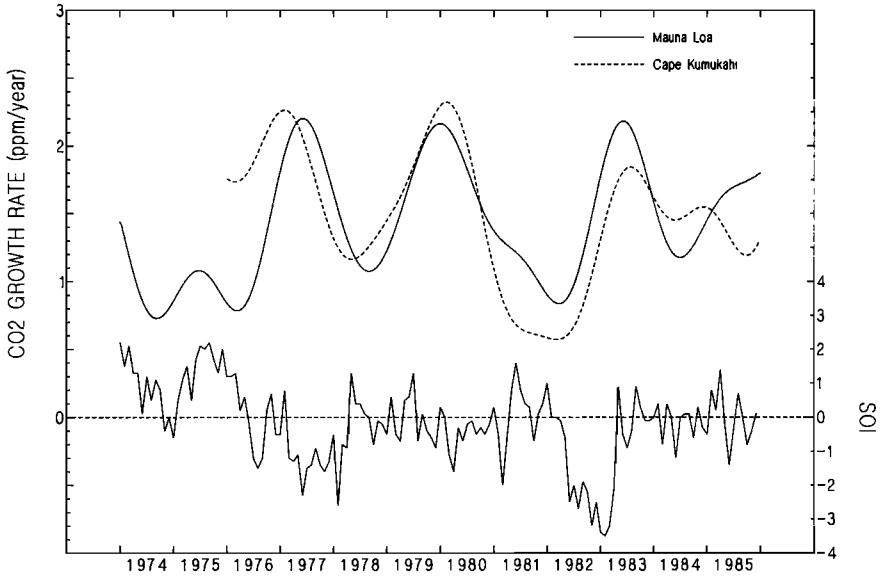

Fig. 12. Growth rate of CO_2 for Mauna Loa (solid curve) and Cape Kumukahi (dashed curve), and monthly values of the Southern Oscillation Index (SOI).

TABLE 4. Fossil Fuel Airborne Fractions

Year	CO_2 Increase, ppm yr^{-1}		Airbornre Fraction, %
	Emission*	Measured†	
1974-1975	2.21	0.92	41.6
1975-1976	2.20	0.99	45.0
1976-1977	2.32	1.10	47.4
1977-1978	2.39	2.03	84.9
1978-1979	2.41	1.23	51.0
1979-1980	2.52	1.77	70.2
1980-1981	2.48	1.81	73.0
1981-1982	2.41	1.16	48.1
1982-1983	2.40	1.11	46.3
1983-1984	2.38	1.99	83.6
1984-1985	2.51	1.30	51.8
1974-1985	26.23	15.41	58.7

*The concentration increase calculated from the total CO_2 emissions from fuels and cement [*Rotty*, 1987, Table 2].

†The difference of the value of the trend line on January 1 of each year.

ppm to the trend data for 1977-1984 that was found for the smoothed data and an uncertainty of 0.32 ppm for 1976 and 1985. The detrended Cape Kumukahi seasonal cycle is shown in Figure 9*b*.

The seasonal cycle characteristics for Cape Kumukahi are listed in Table 5. The uncertainty of each amplitude value is estimated to be 0.42 ppm (one standard deviation) for 1977-1984, and 0.55 ppm for 1976 and 1985. The average amplitude for Cape Kumukahi is 8.38 ± 0.49 ppm, which is 1.55 ppm (23%) larger than Mauna Loa for the same period. We have not found a significant increase in the seasonal amplitude with time (0.063 × 0.052 ppm yr^{-1}). The uncertainties in the parameters for the seasonal cycle at Cape Kumukahi are a factor of 2 larger than the uncertainties for Mauna Loa. Part of this is because the sampling frequency is much less at Kumukahi, and a flask sample is not necessarily a good estimate of the daily mean CO_2 concentration. In addition, the first half of the Kumukahi flask record for 1980 was contaminated and replaced with interpolated data points [*Komhyr et al.*, 1985]. It appears that the interpolated data points were too low, resulting in an anomolously low amplitude for that year. The amplitude for 1977 is also smaller than usual, but there is no obvious problem with the data that might account for this.

The phase of the Kumukahi seasonal cycle is different from Mauna Loa, with the average trend-crossing date during uptake on January 9 and the average trend-crossing date during drawdown on July 16. The differences in the amplitude and phase of the cycle can be seen more clearly by plotting the average seasonal cycles for Mauna Loa and Cape Kumukahi together (Figure 14). Cape Kumukahi has a larger and earlier maximum with a steeper drawdown and earlier summer minimum. This may be attributed to the strong biospheric uptake of CO_2 at low elevations, with the signal at the higher elevation of Mauna Loa attenuated and delayed owing to the vertical transport of CO_2in the atmophere. Mauna Loa is generally lower in concentration than Cape Kumukahi, except during the summer months.

During the afternoon dip at Mauna Loa, air is brought up the mountain from lower elevations and the CO_2 concentration decreases. This dip in concentration occurs throughout the year, and varies in magnitude and frequency of occurrence. Since the data record at Cape Kumukahi shows that the air at sea level is higher in CO_2 concentration than Mauna Loa for most of the year, depletion of CO_2 must be occurring when the air passes over the vegetation at lower elevations. The vertical gradient (Mauna Loa minus Kumukahi) runs from about -1 ppm in winter to about +2 ppm in summer. However, the diurnal cycle plots in Figure 2 show the average magnitude of the diurnal dip to be about 0.5-1 ppm in winter and only about 1.5 ppm in summer. We feel that the values shown in Figure 2 underestimate the actual magnitude of the afternoon drawdown, since examination of plots of hourly CO_2 data shows that the dips can be as large as 4 ppm during August and September.

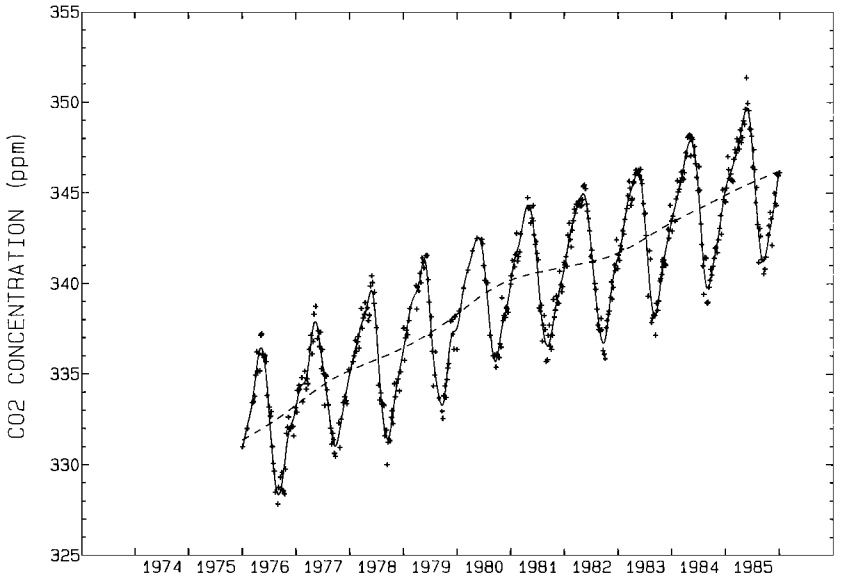

Fig. 13. Cape Kumukahi CO_2 flask data. The crosses represent the flask values. The smooth solid curve is obtained by filtering the data with a cutoff point at 83 days. The dashed curve is obtained by filtering with a 667-day cutoff point.

TABLE 5. Seasonal Amplitude Characteristics of CO_2 at Kumukahi

Year	Maximum	Max DOY	Minimum	DOY	Amplitude	Cross	
						+	–
1976	4.48	127	-4.26	253	8.74	22	190
1977	3.82	132	-3.80	272	7.62	6	202
1978	3.92	152	-4.63	257	8.55	12	201
1979	4.26	144	-4.45	263	8.71	4	193
1980	3.36	143	-4.13	262	7.49	24	206
1981	3.85	120	-4.19	253	8.04	8	190
1982	3.85	126	-4.70	266	8.55	7	196
1983	3.96	132	-4.66	251	8.62	13	195
1984	3.98	124	-4.66	250	8.64	-2	194
1985	4.25	143	-4.65	255	8.90	-3	199
Average	3.99	134	-4.39	258	8.39	9	197
s.d.	0.32	11	0.31	7	0.49	9	5

Maximum and minimum refer to largest deviation from trend line in parts per million. Amplitude equals maximum minus minimum. Max DOY and Min DOY are dates of maximum and minimum in day of year. Cross plus and minus signs refer to the day of year where seasonal cycle crosses the trend line; s.d. is one standard deviation about the average.

These facts suggest that the amount of CO_2 depletion in the air caused by the vegetation is of the order of 1-2 ppm, which when combined with the vertical gradient in CO_2 gives approximately the correct value for the diurnal dip observed at Mauna Loa.

The growth rate of CO_2 at Cape Kumukahi is shown as the dashed line in Figure 12. It has the same general shape as the Mauna Loa growth rate, with small differences in the magnitude and timing. The average growth rate for Cape Kumukahi for 1976 through 1985 was 1.48 ppm yr^{-1} which is not significantly different from the Mauna Loa value of 1.51 ppm yr^{-1} for the same period. The minimum growth rate in 1982 is less at Cape Kumukahi than at Mauna Loa, with the following maximum in 1983 also less at Kumukahi than at Mauna Loa. This would seem to indicate a change in the concentration difference between the two sites. The trend line for Mauna Loa, which is lower than the trend line for Kumukahi before 1982, crosses over the Kumukahi trend line at the end of 1982 and remains higher through the end of 1985.

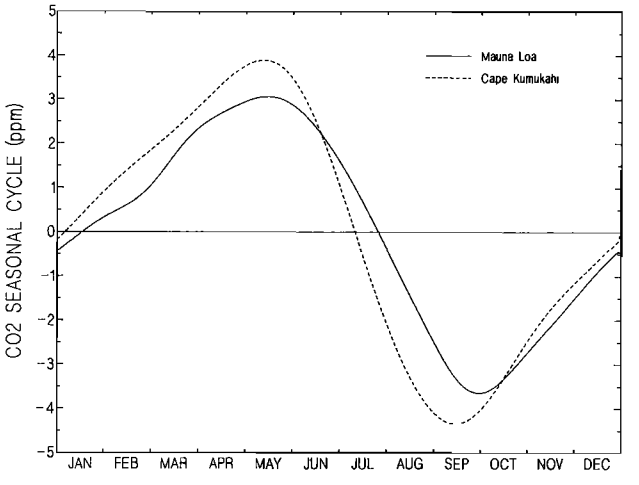

Fig. 14. Average seasonal amplitude for Mauna Loa (solid curve) and Cape Kumukahi (dashed curve). The curves have been obtained by averaging the individual years shown in Figure 9.

6. CONCLUSIONS

This paper describes the first 12 years (1974-1985) of continuous atmospheric CO_2 concentration measurements from the NOAA GMCC program at the Mauna Loa Observatory in Hawaii. Continuous measurements have the advantage that the short-term variations in CO_2 concentration are well determined, so that a consistent selection of the data for baseline conditions is possible, even at a relatively noisy site such as Mauna Loa (compared to some southern hemisphere sites, for example). For the various derived parameters we calculated the statistical uncertainties that arise both from the atmospheric variability (noise) in the data as well as that due to the filtering techniques involved. The uncertainties for Mauna Loa were consistently lower than the uncertainties for the parameters derived from the flask sampling program at Cape Kumukahi. There are also features in the data that can only be determined with the high frequency sampling and subsequent analysis (using hourly and daily averages in our case) that is possible with continuous measurements. For example, there is a significant band of frequencies with periods of 1-2 weeks in the power spectrum of the Mauna Loa data that cannot be seen when sampling at weekly intervals with flasks or when using weekly or monthly averages.

The seasonal amplitude at Mauna Loa was found to be increasing at a rate of 0.05 ± 0.02 ppm yr^{-1} . The average growth rate was 1.42 ± 0.02 ppm yr^{-1} . The airborne fraction for 1974 through 1984 was 58.7%. The Mauna Loa seasonal cycle was found to have a smaller amplitude and a phase lag with respect to the cycle determined from flask sampling at sea level at Cape Kumukahi. Also, the mean concentration at Mauna Loa is less than at Cape Kumukahi. This leads to a seasonally varying vertical gradient between the sea level and the high-altitude sites. Only minor differences were found in the growth rates between Mauna Loa and Cape Kumukahi for the years 1976-1985.

Acknowledgments. We want to thank Ranjit Passi and John Flueck (NOAA Statistics and Applied Mathematics, Boulder) for their helpful discussions about the power spectrum and the autocorrelation in the Mauna Loa data. We also thank T. J. Conway (GMCC) for numerous

and helpful comments on the text, and J. F. S. Chin for his diligent efforts in operating the CO_2 analyzer system at Mauna Loa for the full course of the record.

REFERENCES

Bacastow, R. B., Modulation of atmospheric carbon dioxide by the Southern Oscillation, *Nature*, 116-118, 1976.

Bacastow, R. B., Influence of the southern oscillation on atmospheric carbon dioxide, in *The Fate of Fossil Fuel CO_2 in the Oceans* (edited by N. R. Anderson and A. Malahoff, pp. 33-43, Plenum, New York, 1977.

Bacastow, R. B., J. A. Adams, C. D. Keeling, D. J. Moss, and T. P. Whorf, Atmospheric carbon dioxide, the Southern Oscillation, and the weak 1975 El Niño, *Science, 210*, 66-68, 1980.

Bacastow, R. B., C. D. Keeling, and T.P. Whorf, Seasonal amplitude increase in atmospheric CO_2 concentration at Mauna Loa, Hawaii, 1959-1982, *J. Geophys. Res., 90*, 10,529-10,540, 1985.

Bevington, P. R., *Data Reduction and Error Analysis for the Physical Sciences*, McGraw-Hill, New York, 1969.

Bischof, W., Carbon dioxide concentration in the upper troposphere and lower stratosphere, II, *Tellus, 23*, 559-561, 1971.

Bloomfield, P., *Fourier Analysis of Time Series: An Introduction*, John Wiley, New York, 1976.

Bolin, B., and W. Bischof, Variations of the carbon dioxide content of the atmosphere in the northern hemisphere, *Tellus, 22*, 431-442, 1970.

Cleveland, W. S., A. E. Freeny, and T. E. Graedel, The seasonal component of atmospheric CO_2: Information from new approaches to the decomposition of seasonal time series, *J. Geophys. Res., 88*, 10,934-10,946, 1983.

Climate Analysis Center, Climate Diagnostics Bulletin: March 1986, Natl. Meteorol. Cent., Natl. Weather Serv., Natl. Oceanic and Atmos. Admin., Washington, D.C., 1986.

Conway, T. J., P. P. Tans, L. S. Waterman, K. W. Thoning, K. A. Masarie, and R. H Gammon, Atmospheric carbon dioxide measurements in the remote global troposphere, 1981-1984, *Tellus, 40B*, 81-115, 1988.

Czeplak, G., and C. Junge, Studies of interhemispheric exchange in the troposphere by a diffusion model, *Adv. Geophys., 18B*, 57-72, 1974.

Enting, I. G., The interannual variation in the seasonal cycle of carbon dioxide concentration at Mauna Loa, *J. Geophys. Res., 92*, 5497-5504, 1987.

Gillette, D. A., W. D. Komhyr, L. S. Waterman, L. P. Steele, and R. H. Gammon, The NOAA/GMCC continuous CO_2 record at the south pole, 1975-1982, *J. Geophys. Res.*, 92, 4231-4240, 1987.

Halter, B. C., and J. T. Peterson, On the variability of atospheric carbon dioxide concentration at Barrow, Alaska, during summer, *Atmos. Environ., 15*, 1391-1399, 1981.

Halter, B. C., and J. M. Harris, On the variability of atmospheric carbon dioxide concentration at Barrow, Alaska, during winter, *J. Geophys. Res., 88*, 6858-6864, 1983.

Halter, B. C., J. M. Harris, and K. A. Rahn, A study of winter variability in carbon dioxide and arctic haze aerosols at Barrow, Alaska, *Atmos. Environ., 19*, 2033-2037, 1985.

Herbert, G. A., E. R. Green, J. M. Harris, G. L. Koenig, S. J. Roughton, and K. W. Thaut, Control and monitoring instrumentation for the continuous measurement of atmospheric CO_2 and meteorological variables, *J. Atmos. Oceanic Technol., 3.*, 416-421, 1986.

Keeling, C. D., R. B. Bacastow, A. E. Bainbridge, C. A. Ekdahl, P. R. Guenther, L. S. Waterman, and J. F. S. Chin, Atmospheric carbon dioxide variations at Mauna Loa Observatory, Hawaii, *Tellus, 28*, 538-551, 1976.

Keeling, C. D., R. B. Bacastow, and T. P. Whorf, Measurements of the concentration of carbon dioxide at Mauna Loa Observatory, Hawaii, in *Carbon Dioxide Review: 1982*, edited by W. C. Clark, pp. 377-385, Oxford University Press, New York, 1982.

Keeling, C. D., T. P. Whorf, C. S. Wong, and R. D. Bellagay, The concentration of atmospheric carbon dioxide at Ocean Weather Station P from 1969 to 1981, *J. Geophys. Res.*, 90, 10,511-10,528, 1985.

Keeling, C. D., P. R. Guenther, and T. P. Whorf, Daily averaged concentrations of atmospheric carbon dioxide at fixed land stations and from air collection over the oceans, Carbon Dioxide Inf. Cent., Oak Ridge, Tenn., 1986.

Komhyr, W. D., and T. B Harris, Measurements of atmospheric CO_2 at the U.S. GMCC baseline stations, Air Pollution Measurement Techniques, *Spec. Environ. Rep. 10, WMO 460*, pp. 9-19, World Meteorol. Organ., Geneva, Switzerland, 1977.

Komhyr, W. D., R. H. Gammon, T. B. Harris, L. S. Waterman, T. J. Conway, W. R. Taylor, and K. W. Thoning, Global atmospheric CO_2 distributions and variations from 1968-1982 NOAA/GMCC CO_2 flask-sample data, *J. Geophys. Res., 90*, 5567-5596, 1985.

Komhyr, W. D., T. B. Harris, L. S. Waterman, J. F. S. Chin, and K. W. Thoning, Atmospheric carbon dioxide measurements at Mauna Loa Observatory, 1, NOAA GMCC measurements with a nondispersive infrared analyzer, 1974-1985, *J. Geophys. Res.*, this issue.

Koopmans, L. H., *The Spectral Analysis of Time Series*, Academic, San Diego, Calif., 1974.

Mendonca, B. G., Local wind circulation on the slopes of Mauna Loa, *J. Appl. Meteorol., 8*, 533-541, 1969.

Miller, J. (Ed.), Mauna Loa Observatory, A 20th anniversary report, Air Resour. Lab., Natl. Oceanic and Atmos. Admin., Silver Spring, Md., 1978.

Miller, J. M., and J. F. S. Chin, Short-term disturbances in the carbon dioxide record at Mauna Loa Observatory, *Geophys. Res. Lett., 5*, 669-671, 1979.

Pales, J. C., and C. D. Keeling, The concentration of atmospheric carbon dioxide in Hawaii, *J. Geophys. Res., 70*, 6053-6076, 1965.

Pearman, G. I., and D. J. Beardsmore, Atmospheric carbon dioxide measurements in the Australian region: Ten years of aircraft data, *Tellus, 36B*, 1-24, 1984.

Pearman, G. I., and P. Hyson, The annual variation of atmospheric CO_2 concentration observed in the northern hemisphere, *J. Geophys. Res., 86*, 9839-9843, 1981.

Peterson, J. T., W. D. Komhyr, T. B. Harris, and J. F. Chin, NOAA carbon dioxide measurements at Mauna Loa Observatory, 1974-1976, *Geophys. Res. Lett., 4*, 354-356, 1977.

Peterson, J. T., W. D. Komhyr, T. B. Harris, and L. S. Waterman, Atmospheric carbon dioxide measurements at Barrow, Alaska, 1973-1979, *Tellus, 34*, 166-175, 1982.

Peterson, J. T., W. D. Komhyr, L. S. Waterman, R. H. Gammon, K. W. Thoning, and T. J. Conway, Atmospheric CO_2 variations at Barrow, Alaska, 1973-1982, *J. Atmos. Chem., 4*, 491-510, 1986.

Reinsch, C. H., Smoothing by spline functions, *Numer. Math., 10*, 177-183, 1967.

Rotty, R. M., A look at 1983 CO_2 emissions from fossil fuels (with preliminary data for 1984), *Tellus, 39B*, 203-208, 1987.

Sadler, J. C., C. S. Ramage, and A. M. Hori, Carbon dioxide variability and atmospheric circulation, *J. Appl. Meteorol., 21*, 793-805, 1982.

Tanaka, M., T. Nakazawa, and S. Aoki, Time and space variations of tropospheric carbon dioxide over Japan, *Tellus*, 39B, 3-12, 1987.

Thompson, M. L., I. G. Enting, G. I. Pearman, and P. Hyson, Interannual variation of atmospheric CO_2 concentration, *J. Atmos. Chem., 4*, 125-155, 1986.

Trenberth, K. E., Seasonal variations in global sea level pressure and the total mass of the atmosphere, *J. Geophys. Res., 86*, 5238-5246, 1981.

Wong, C. S., Y.-H. Chan, J. S. Page, R. D. Bellegay, and K. G. Pettit, Trends of atmospheric CO_2 over Canadian WMO background stations at Ocean Weather Station P, Sable Island, and Alert, *J. Geophys. Res., 89*, 9527-9539, 1984.

World Meteorological Organization, Climatic change, *WMO Tech. Note 79*, Geneva, Switzerland, 1966.

W. D. Komhyr, Air Resources Laboratories, R/E/AR4, Environmental Research Laboratory, NOAA, 325 Broadway, Boulder, CO 80303.

P. P. Tans and K. W. Thoning, Cooperative Institute for Research in Environmental Sciences, University of Colorado, Boulder, CO 80309.

(Received June 10, 1988;
revised February 10, 1989;
accepted February 10, 1989.)